RSC Advances

PAPER

View Article Online
View Journal | View Issue

Cite this: *RSC Adv.*, 2025, **15**, 43877

Grafting ethanedithiol moiety on the surface of cellulosic fibers by thioesterification: a simple chemical method

Md. Sadiqul Islam Sheikh,† Md. Rezanur Rahman, Muhammed Shah Miran, Md. Abu Bin Hasan Susan and Md. Mominul Islam *

Jute fibers (JFs), in which two-thirds of their total mass is cellulose, are valuable bio-fibers employed from the household to technical applications in the environmental, pharmaceutical, and energy storage fields. However, their poor interfacial adhesion with polymer matrices hinders their widespread industrial application, particularly in composite materials. In this study, JFs were modified by grafting thiol moieties through mild oxidation, followed by esterification in an aqueous solution to enhance their functional performance and broaden their industrial utility. First of all, JFs were collected from a local market and pretreated with an alkali solution and oxidized with 20% Fenton reagent (FR). The desired grafting of thiol moieties was achieved by refluxing the initially oxidized JFs with ethane-1,2-dithiol in acetonitrile using trifluoroacetic acid as a catalyst at 60 °C for 4 h. These materials were characterized by Fourier-transform infrared spectroscopy, conductometric titration, thermogravimetric analysis, X-ray diffraction, scanning electron microscopy, fiber strength and contact angle analyses. The characteristic features of the –COOH groups and conductometric titration confirmed that the amount of –COOH groups decreased after thioesterification, as expected. The degree of oxidation of cellulose on the fiber surface was about 4.5%. The changes in crystallinity, surface morphology, tensile strength, and thermal stability support the efficient grafting of thiol moieties on the surface of JFs. The absorption bands corresponding to the –C=O and –C(=O)–S– groups in the FT-IR spectra suggested the desired modification. 20% FR was sufficient for introducing a significant amount of these groups (280.39 μmol g^{-1}). The increased hydrophobicity of the thiol-grafted JFs, as evaluated by contact angle measurements, evidenced the expected modification. With this enhanced surface functionality, the modified JFs show potential for applications in heavy metal remediation, industrial dye removal, wastewater treatment, and composite reinforcement, offering a sustainable and eco-friendly solution to environmental and industrial challenges.

Received 9th October 2025
Accepted 15th October 2025

DOI: 10.1039/d5ra07729j

rsc.li/rsc-advances

1. Introduction

Global environmental concerns, such as melting polar icebergs, global warming, fast-depleting petroleum resources, and increasing sea levels, have transformed the use of plastics and synthetic materials in the direction of natural-based biopolymers, which are biodegradable, completely sustainable, and environmentally friendly.[1,2] Owing to environmental protection as well as government legislation in different countries, non-wood plant fibers with a short growth cycle have become more important than the utilization of wood fibers from growing trees. Cellulose, the most abundant natural biopolymer, has received increasing attention because of its high barrier properties, high specific surface area, high strength, low thermal expansion, lightweight, and biodegradability.[3–8] As a source of cellulose, jute fibers (JFs) have become a promising research focus due to their availability, low cost, and high cellulose content, which make them ideal for various chemical modifications. Additionally, JFs are a renewable and biodegradable resource, making them an environmentally sustainable candidate for advanced material applications.

Besides their common uses, JFs have immense potential in technical applications including wastewater treatment, water ultrafiltration, and energy storage devices.[9] These applications are supported by their mechanical properties, including tensile strength, specific strength, and modulus.[10,11] As a typical kind of non-wood fiber, jute is a low-cost multicellular and lignocellulosic fiber widely cultivated in Asian countries, such as China, India, and Bangladesh, and it can be harvested in large quantities annually.[12,13] JFs consist of cellulose (64.4%), hemicellulose (12.0%), lignin (11.8%), a small amount of pectin, vegetable wax, and other components.[14] The higher cellulose

Department of Chemistry, University of Dhaka, Dhaka-1000, Bangladesh. E-mail: mominul@du.ac.bd

† Department of Chemistry, Khulna University of Engineering & Technology, Khulna-9203, Bangladesh.

content (45–71.5%) and crystallinity (especially higher than other non-wood fibers) of JFs make it suitable for the fabrication of cellulose nanowhiskers (CNWs).[15] In JFs, the cellulose molecules are highly oriented parallel to each other in fibrils, thus reducing their degree of orientation parallel to the fiber.[16] The microfibril angle (7°–12°) of JFs is relatively larger than that of the other bast fibers (*e.g.* flax, ramie, and hemp), which is favorable for the extraction of cellulose nanofibers (CNF) from JFs.[17]

The isolation of CNF mainly from JFs has been investigated by many researchers. The basic approaches for the extraction of CNF from JFs are mainly categorized as acid hydrolysis, catalytic oxidation, and steam explosion.[18–20] A facile method for generating CNF with tunable polymorphs and crystallinity has been reported, which involves the alkali treatment of JFs, followed by TEMPO-mediated oxidation and mechanical disintegration. The resulting CNF retain the cellulose polymorph of the source material but exhibit a significantly higher crystallinity index.[19] CNW were fabricated from JFs using a TEMPO/NaBr/NaClO system for selective oxidation combined with mechanical homogenization, producing a mass with ultrathin diameters (3–10 nm) and high crystallinity (69.72%).[12] Highly carboxylated cellulose nanocrystals were derived from JFs *via* facile oxidation with ammonium persulfate. They exhibited greater crystallinity and improved thermal stability compared to the virgin JFs.[21] Microcrystalline cellulose was prepared from JFs using formic acid and the peroxy formic acid process, followed by acid hydrolysis. It showed greater thermal stability and crystallinity than the untreated fibers.[22] Isolation of bionanowhiskers from jute by alkali treatment followed by acid hydrolysis has been studied. A rod-like morphology was observed, which might be useful as a reinforcing phase in nanocomposites.[23]

The grafting of suitable compounds with the hydroxyl groups located on the cellulose backbone is one of the prime approaches for modifying the physical and chemical properties of JFs. The surface properties of JFs can be tuned by modification. The grafting modification of JFs has been attempted by many researchers, which fall into two major types of chemical methods and physical methods. Chemical methods using initiators such as ceric ions, V^{5+}-cyclohexanone system, $K_2S_2O_8$, laccase/TEMPO system, and Fe^{2+}/H_2O_2 system have been reported for the grafting of different synthetic monomers onto JFs.[24–28] The grafted samples exhibited better thermal stability, light fastness, mechanical properties, and dye fixation compared to the pristine ones. Physical methods such as plasma treatment, UV radiation, gamma radiation, and combined UV and gamma radiation have been employed for grafting different acrylate and polylactic acid onto JFs.[29–32] The tensile modulus, flexural strength, and elongation at the break of the grafted JFs were found to be enhanced compared to that of the virgin JFs.

Thiol-modified natural fibers and their composites have diverse applications, including drug delivery, tissue engineering, pharmaceuticals, wastewater treatment, heavy metal remediation, water detoxification, and energy storage devices. These applications have attracted significant research interest in the field of cellulose-based materials.[2,10,33] Several strategies have been explored to enhance the properties of JFs through chemical or biochemical modification. Acosta Ortiz *et al.* employed a thiol–ene photopolymerization approach to fabricate woven JF/epoxy biocomposites, where thiol functionalities were exploited mainly to achieve surface crosslinking within the polymer matrix, thereby improving the performance of the composite.[34] In contrast, the enzymatic-assisted grafting of vinyl copolymers onto jute fabrics has been reported to impart durable hydrophobicity.[35] This method relies on enzymatic catalysis and vinyl monomers to generate functional polymer coatings rather than directly modifying cellulose.[35] Similarly, El-Shafei *et al.* developed dual-functional jute fabrics by integrating chitosan and phosphorylated nanocellulose, producing antimicrobial activity and enhanced thermal stability suitable for biocomposite applications.[36] However, to the best of our knowledge, no relevant attempt and analysis have been made to graft thiols onto JF *via* a thioesterification reaction to date. Moreover, reactive oxygen species (ROS) including hydrogen peroxide (H_2O_2), $OH^{\bullet}$, and superoxide are environmentally friendly, cost-effective, and readily accessible oxidizing agents for the oxidation of cellulose.[1] Among them, $OH^{\bullet}$, a highly reactive species, can be easily formed from H_2O_2 *via* a Fenton or photo-Fenton process. Given that after treatment, the ROS family leaves O_2 and water as green by-products, they have been employed as clean reagents for practical applications over the TEMPO system.[37]

Various chemical modifications of JFs have been reported, including silanization, acetylation, and maleation.[38–40] In contrast, only a limited number of studies have explored mild thioesterification to introduce functional –SH groups without requiring metal catalysts or multistep synthesis. This relatively unexplored method enhances the functionality of fibers and opens new prospects for advanced applications in composite materials and environmental remediation. Thiol groups were grafted onto JFs *via* thioesterification because of their strong binding affinity for heavy metal ions and organic pollutants. This approach offers distinct advantages for sustainable, bio-based applications, including wastewater treatment, bio-adsorbents, water filtration, and composite reinforcement.[1,33,41] Hemicellulose, lignin, pectin, and other waxy substances were removed first by the reaction of JFs with alkali. Simple oxidation of fibers was carried out to introduce –COOH groups utilizing FR in an aqueous solution as a green route. Thioesterification of oxidized JFs was carried out using dithiols in mixed organic and aqueous media *via* different methods.[1,42,43] These materials were characterized by FTIR spectroscopy, conductometric titration, thermogravimetric analysis, XRD, SEM, and fiber strength and contact angle analyses. JFs as a source of cellulose from non-wood plants, could be derivatized with thioester groups using this straightforward modification approach.

2. Experimental

2.1. Materials

Fibers extracted from the jute plant (*Corchorus olitorius*) were purchased from the local market. Acetonitrile (CH_3CN, Sigma-

Aldrich, USA, purity 99.5%), ethane-1,2-dithiol ($HSCH_2CH_2SH$, Sigma-Aldrich, USA, purity ≥99.0%), ferrous sulfate heptahydrate ($FeSO_4 \cdot 7H_2O$, Unichem, India, purity 98.5%), hydrogen peroxide (H_2O_2, Scharlau, Spain, purity 98.0%), sodium hydroxide (NaOH, Merck, India, purity ≥97.0%), sulphuric acid (H_2SO_4, Sigma-Aldrich, USA, purity 99.0%), toluene (Sigma-Aldrich, USA, purity 99.3%), and trifluoro acetic acid (CF_3-COOH, Sigma-Aldrich, USA, purity 99.0%) were used as received without any further purification. De-ionized water (specific conductance <0.1 μS cm^{-1}) prepared with a water purifier (BOECO pure, model-BOE 8082060, Germany) was used throughout the study.

2.2. Preparation of jute samples

The JFs were cut into a finite size of 3 cm in length. A weighed amount of sample was added to a 500 mL beaker and washed thoroughly 3–4 times with de-ionized water to eliminate dust particles and other water-soluble impurities. Then, the fibers were initially dried for approximately 8 h in open air, and finally oven-dried at 40 °C for 4 h.

2.2.1. Preparation of Fenton reagent. FR solution was prepared according to the procedure reported in the literature.[1,44] Typically, the preparation of 20% FR was accomplished by mixing 0.02 g of solid $FeSO_4$, 1.0 mL of 0.1 M H_2SO_4, and the remaining volume of 20% H_2O_2 solution. In a solution of higher pH, Fe^{2+} ions are prone to precipitate as $Fe(OH)_3$, reducing the effectiveness of the FR solution. Thus, the pH of the solution was adjusted to be less than 3. A fixed concentration (20% FR) of FR based on the literature was maintained because it yielded the highest number of carboxylic acid groups on the JFs.[1] The generation of carboxylic acid functionalities is a critical step in enhancing the reactivity of cellulose for subsequent thioesterification reactions.

2.2.2. Alkalization process. Alkalization of JFs is normally carried out for the removal of noncellulosic substances such as hemicellulose, lignin, and pectin, which was carried out according to the literature.[44] Typically, 10.0 g of dried JFs was soaked in 5% of NaOH solution in a 500 mL beaker, and then the mixture was heated at 80 °C for 4 h. After that, the JFs were removed from the reddish-brown color alkaline mixture. These fibers were washed with de-ionized water 3–4 times. The mass was first dried in open air for about 8 h, then placed in an oven at 40 °C for 4 h, and the final weight was subsequently recorded. The obtained NaOH-treated JFs were named NJF.

2.2.3. Oxidation of jute fibers. The JFs were oxidized with 20% FR to introduce carboxylic groups in the cellulose moieties by following the literature.[1,44] It has been reported that out of 12 different concentrations of three reactive oxygen species such as H_2O_2, FR, and peroxyacetic acid, 20% FR is the strongest oxidizing agent given that it introduces the highest number of carboxylic groups in the cellulose backbone by oxidation reaction.[1] Hence, 20% FR was utilized to oxidize the cellulose in JFs. Typically, 1.0 g of NJF was treated with 80 mL of 20% FR solution. The reaction was performed at room temperature for 12 h. A magnetic stirrer bar was used for mixing at 200 rpm to ensure uniform and good mixing. Then, the mixture was filtered through a Büchner funnel using Whatman filter paper to separate the oxidized JFs (OJF). The fibers were subsequently washed with ~300 mL of de-ionized water until the filtrate reached neutral pH (6.5–7.0), confirming the removal of residual acid and Fenton reagent components. The samples were air-dried for approximately 8 h, followed by oven drying at 40 °C for 4 h, and then their weights were recorded.

2.2.4. Thioesterification of OJF. The two strategies known as Method I and Method II, as described in the literature, were employed to accomplish the thioesterification of OJF.[1,42] In brief, a single-necked 100 mL round-bottomed flask fitted with a magnetic stir bar and connected to a reflux condenser was charged with 1.0 g of OJF and 0.5 mL of ethanedithiol in 30 mL of solvent. The solvent was a mixture of toluene and water in a weight ratio of 4 : 1, which was chosen based on experimental observation. The fibers showed better dispersion in this mixture, as confirmed by visual inspection, ensuring a uniform suspension for the reaction. The fibers were dispersed by sonication for 30 min before adding the reagents. To enhance the equilibrium reaction of carboxylic acid and ethanedithiol and the product (thioester), as represented in Scheme 1, 1.0 mL of 1.0 M H_2SO_4 was used as a Brønsted acid-catalyst. The whole setup was placed in a water bath and subjected to constant stirring at 85 °C for 6 h. The resulting mixture was cooled to room temperature. After completion of the reaction, the mixture was filtered and washed several times with acetone and ethanol. Then, the thioesterified JFs (TJF-I) were first air-dried for about 8 h, then oven-dried at 40 °C for 4 h, and finally their weights were measured.

A major portion of the synthetic process adopted in Method II is analogous to Method I. However, acetonitrile was used as the solvent in the former, whereas trifluoroacetic acid was used as the catalyst in the latter case.[1,43] Initially, trifluoroacetic acid was added drop-wise to the stirred mixture over 15 min at room temperature and allowed to react at 60 °C for 4 h. The final products were denoted as TJF-II. A schematic representation of the alkalization, oxidation, and thioesterification of cellulose of JF is depicted in Scheme 1.

2.3. FT-IR spectral analysis

FT-IR analysis of the pellet of the raw, alkali-treated, oxidized and thioesterified JFs was performed using an FT-IR (PerkinElmer, USA, Frontier FT-IR/NIR) system. Spectra were recorded in the range of 4000–400 cm^{-1}. The number of scans was 32 and the resolution was 4 cm^{-1}. Typically, 0.5 mg of fibers was ground into a fine powder using an agate mortar, and then mixed with 100 mg of KBr to prepare the pellet. Finally, a 5-ton pressure was applied to form the pellet in a metal holder. The pellet was then placed in the sample holder of the FT-IR spectrometer. The intensity of the sample beam and the reference beam was monitored using a thermocouple detector, and the final data output can be displayed in either transmittance or absorbance mode and expressed by eqn (1), as follows:

$$\text{Transmittance} = \frac{I_s}{I_r} \times 100\% \quad (1)$$

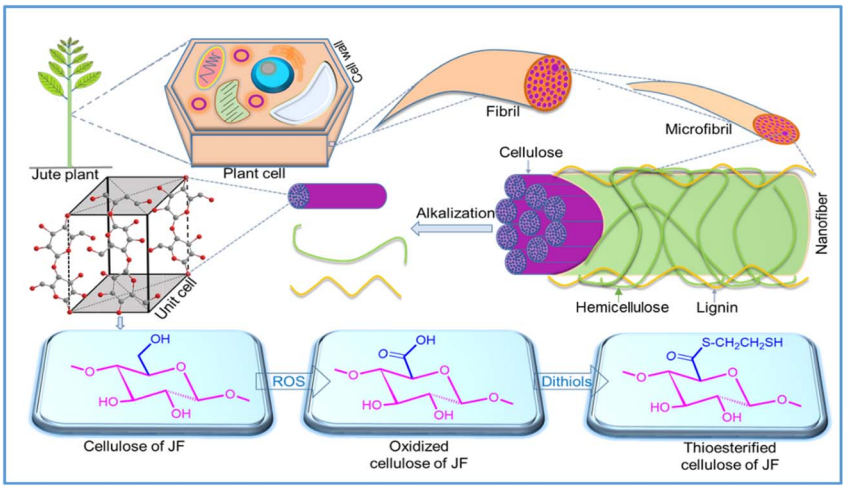

Scheme 1 Illustration representing the functionalization of cellulose on the surface of JF *via* oxidation and thioesterification.

where I_s and I_r refer to the intensity of the sample beam and reference beam, respectively. The FT-IR spectra were further analyzed by deconvolution using Gaussian peak fitting to resolve the overlapping bands. The GaussAmp function was employed to extract overlapping peaks and correct the baseline of the spectra.

2.4. SEM analysis

The morphology of the jute-based samples was determined by scanning electron microscopy (Model: JEOL, JSM-7600F, USA). The acceleration voltage of the electron gun was 5 kV with a probe current of 1.0 nA. A small amount of the powder sample was uniformly dispersed onto carbon tape attached to an aluminum SEM stub. The specimens were then coated with a thin (~20 Å) layer of gold using a vacuum sputter coater to prevent surface charging during analysis. Prior to imaging, the samples were analyzed under high-vacuum conditions. Secondary electron images were captured at magnifications between 100× and 5000× to evaluate the particle morphology, surface features, and agglomeration.

2.5. Conductometric titration

The carboxyl content in OJF and its corresponding grafted samples was determined by conductometric titration.[1,45] Approximately 50 mg sample was suspended in 15 mL of 0.01 M HCl solution. After stirring for 10 min, the suspension was titrated with 0.01 M NaOH. The titration curves display the presence of strong acid, corresponding to the excess HCl depicted as zone 1, weak acid belonging to the carboxyl content of OC assigned as zone 2, and strong base region due to NaOH denoted as zone 3 in Fig. 5. The degree of substitution (DS) can be computed using eqn (2) from the conductometric titration.[46]

$$\mathrm{DS} = \frac{162 \times C \times (V_2 - V_1)}{w - (36 \times C \times (V_2 - V_1))} \times 100\% \quad (2)$$

where C denotes the concentration of NaOH in mol L^{-1}, V_1 and V_2 are the amounts of NaOH in L and w is the weight of the oven-dried sample in g. 162 stands for the molecular weight (g mol^{-1}) of an anhydroglucose unit (AGU) and 36 corresponds to the difference between the molecular weight of an AGU and that of the sodium salt of a glucuronic acid moiety.

2.6. Thermal analysis

A differential thermal analyzer (Hitachi TG/DTA 7200) was employed to examine the thermal stability of the jute-based samples, concurrently maintaining an N_2 atmosphere at a flow rate of 100 mL min^{-1}. In a typical experiment, about 5 mg of sample was placed in a clean ceramic pan and heated from 30 °C to 700 °C for the samples at a rate of 10 °C min^{-1}.

2.7. XRD analysis

The X-ray diffraction patterns of the raw, extracted, oxidized and thioesterified JFs were recorded using an Ultima IV, Rigaku X-ray diffractometer operating at 40 kV and 40 mA using Cu $K_{\alpha 1}$ radiation (λ = 1.5406 Å) fitted with a scintillation detector. The measurement was conducted in continuous mode at a scan speed of 3.0 min^{-1} in the 2θ scan range of 10°–70° with the scan width of 0.02°. The crystallinity index (CI) was calculated using the XRD amorphous subtraction method.[47] The CI was calculated as the ratio of the area of the crystalline domain to the total area using eqn (3), as follows:

$$\mathrm{CI} = \frac{A_{\mathrm{total}} - A_{\mathrm{am}}}{A_{\mathrm{total}}} \quad (3)$$

where A_{total} is the integrated intensity of the diffraction spectrum and A_{am} is the integrated intensity of the amorphous background. In addition, the crystallite size (CS) was determined from XRD data using eqn (4), as follows:[48]

$$\mathrm{CS} = \frac{K\lambda}{\cos\theta} \quad (4)$$

where K is the correction factor (0.9), β is the full width at half maximum in radians, and λ is the wavelength of X-rays and is half of the angle for the corresponding peak. The band was

Table 1 Summary of the results of JF derivatization under different conditions

Reaction/reagents	[a]Material	Yield/%	–COOH group/mmol g^{-1}	[b]DS/%	[c]CI/%	[c]Crystallite size/nm	[c]2θ (°) at max. Intensity	[d]Thermal decomposition		Bundle strength/lb mg^{-1}
								Onset-I/°C	Onset-II/°C	
Unreacted										
Jute fiber (JF)	JF				70.14	6.58	22.24	270	368	1.13
Alkalization										
JF + 5% NaOH, 25 °C	NJF	76.43			72.92	23.01	22.74	270	368	1.02
Oxidation										
FR: (20% H_2O_2 + $FeSO_4$ + H_2SO_4) + JF; 25 °C	OJF	68.55	280.4	4.5	82.67	5.14	22.74	235	300	0.07
Thioesterification										
Method I: H_2SO_4 + $HSCH_2CH_2SH$ + 20% FR-OJF; toluene + water; 85 °C	TJF-I	83.33	10.8	4.3	75.71	6.34	22.70	250	330	
Method II: H_2SO_4 + $HSCH_2CH_2SH$ + 20% FR-OJF; acetonitrile + CF_3COOH; 40 °C	TJF-II	86.84	33.5	4.0	74.39	6.46	22.70	230	295	

[a] Abbreviated name. [b] Conductometric titration. [c] XRD. [d] TG-DTA.

deconvoluted using the GuessApp peak-fitting method to calculate the area under the (110) diffraction peak.

2.8. Determination of tensile strength

The tensile strength of the treated jute samples was determined. The bundle strength (*i.e.*, Pressley index = breaking load (lb)/weight of bundle (mg)) of the fibers in each sample was determined using a Presley fiber strength tester using zero-gauge strength.[44] A flat bundle with a length of approximately 3 cm was held by a pair of clamps. All corner ends of the fibers were then sheared off evenly and tension was applied to separate the clamps, and thereby tear the fibers. The torn bundle was weighed in a precision balance. The resulting strength (Pressley index) was computed from the breaking load in lb and weight of the bundles in mg to determine the tensile strength of the samples under consideration.

2.9. Contact angle measurement

To understand the surface modification of JFs, the surface hydrophilicity of the prepared samples was evaluated by contact angle measurements using a contact angle goniometer (L2004A1, Ossila BV, Netherlands). The sample was dispersed in a mixture of toluene and water in a weight ratio of 4 : 1. The dispersed mixture was sonicated for 30 min before measurement. A drop of the mixture (1–2 μL) was dropped in the center of the vertical tilt stage through a micro-syringe. The region of interest box was adjusted until the entire droplet was within the box. The circle fitting technique was applied to the droplet. The gradient of the fit at the baseline was utilized to estimate the contact angle.

3. Results and discussion

3.1. Modification of jute fibers

The JFs were subjected to different types of chemical reactions to introduce thiol groups in the cellulose moiety. Table 1 presents the % yield of NJF, OJF, TJF-I, and TJF-II, which is 76.43%, 68.56%, 83.34% and 86.84%, respectively. The removal of noncellulosic substances such as hemicellulose, pectin, and a small amount of lignin was performed by treatment of JFs with NaOH. The color of JFs is off-white to brown, while NJF appears as a more intense brown color than that of JFs. NJF was treated with FR to incorporate –COOH groups predominantly at the C6 position, while due to its partial oxidation, aldehyde and ketone groups might also be introduced. Lignin and wax are also detached through FR treatment and oxidation of NJF causes a bleaching effect on the fiber surface. A gradual reduction in hemicellulose and lignin content has been observed, while the cellulose content increased significantly by alkali treatment. For instance, the cellulose content increased to 85.1% with 15% NaOH treatment, confirming the effective removal of noncellulosic components. These findings were supported by FTIR and TGA analyses, which confirmed the removal of lignin and hemicellulose and the improvement in thermal stability.[49] In the present case, the removal of hemicellulose was confirmed by FTIR analysis, as described below. The color of OJF is less

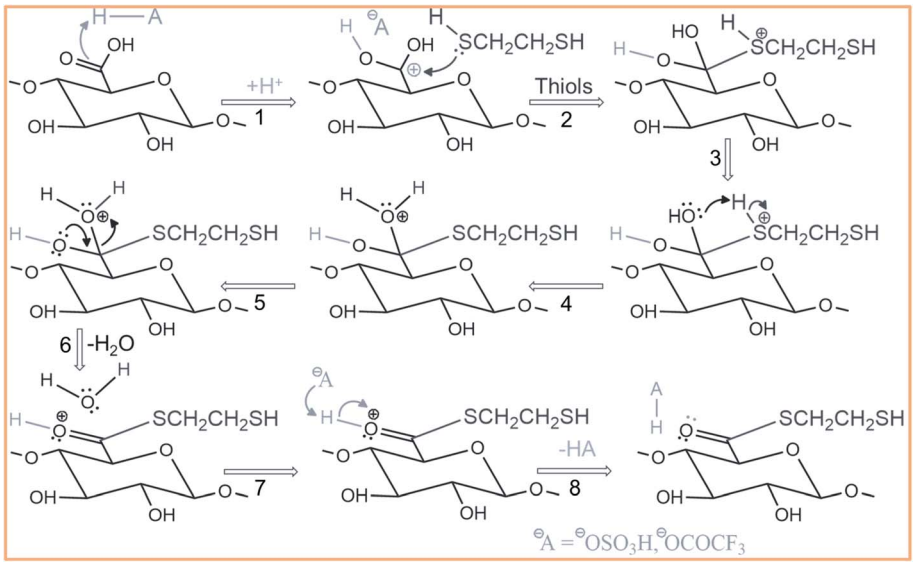

Scheme 2 Proposed mechanism for the thioesterification of OJF. (1) Delocalized carbocation formation, (2) attack by thiol, (3) transfer of a proton, (4) formation of a good leaving group, (5) formation of the pi bond, (6) elimination of water, (7) removal of proton by acid, and (8) thioester formation.

intense than that of NJF. Due to the oxidation of cellulose, β-elimination occurs in the cellulose chain, resulting in a lower % yield of OJF compared to NJF. OJF was reacted with ethanedithiol to prepare the thioesterified JF.[50] This β-elimination did not occur during thioesterification. Thus, the % yield of TJF-I and TJF-II was augmented compared to that of OJF. The surface of TJF-I and TJF-II is pale yellow. TJF-I and TJF-II exhibit a more disintegrated form than that of OJF. Method II shows a higher yield than Method I. Method II likely improves upon Method I by reducing the material losses during the synthesis due to the variable reaction parameters such as time, temperature, and solvent ratios. Furthermore, the reaction temperature of Method II is lower than that of Method I. These optimizations result in the more efficient recovery of the target compounds or materials in Method II. The detailed mechanism of thioesterification of OJF is discerned in Scheme 2.

3.2. Molecular characterization

Fig. 1 presents the FTIR spectra of JFs, NJF, OJF, TJF-I, and TJF-II. This analysis was adopted to evaluate the incorporation of functional groups such as –COOH and –S–CH_2–CH_2–SH into the glucose units present on the surface cellulose of JFs. The strong broad band at around 3400 cm^{-1} is assigned to different –O–H stretching modes. The three bands at around 2944, 2895, and 2842 cm^{-1} are related to the –C–H symmetric stretching of the olefinic group, sp^3 –C–H symmetric stretching vibrations, and sp^3 C–H symmetric stretching of CH_2 groups, respectively. The bands at 1595, 1510, and 1255 cm^{-1} are assigned to –C=C–, –C–O stretching or bending vibrations of the different groups present in lignin, respectively. The band at 1738 cm^{-1} is attributed to the symmetric stretching of the –C=O groups. This band is due to the acetyl group or uronic ester groups of hemicellulose present in the JFs.

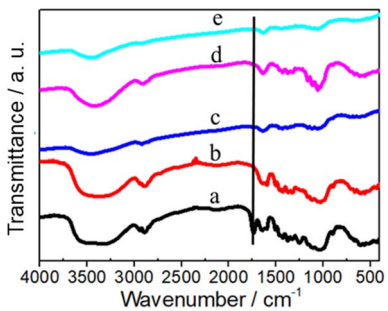

Fig. 1 FT-IR spectra of (a) JF, (b) NJF, (c) OJF, (d) TJF-I, and (e) TJF-II.

The absorption band at 1510 cm^{-1} arises from the aromatic skeletal vibration of –C=C– in the benzene ring, which is characteristic of lignin. The bands at 1460, 1425, 1335, and 1110 cm^{-1} are characteristic of –C–H, –C=O deformation, bending, or stretching vibrations of many groups in lignin, respectively. The absorption bands near 1060 cm^{-1} are attributed to the C–O–C symmetric ring stretching in the cellulose backbone. The characteristic band near 895 cm^{-1} is associated with β-anomers or β-glycosidic linkage in cellulose polymers.[48]

The disappearance of the band at 1738 cm^{-1} in NJF indicates that the hemicellulose in JFs is eliminated through alkali treatment because hemicellulose contains carboxylic groups and is soluble in hot water. During the NaOH treatment of JFs, lignin was also removed to some extent. However, the presence of an absorbance band at 1456 cm^{-1} in NJF is associated with CH_3 deformation in lignin. The bands at 1502 and 1030 cm^{-1}, which are characteristic of lignin, are still observed after the alkalization process, indicating the presence of residual lignin.[51] This demonstrates that hemicellulose is much easier to unveil by alkali treatment compared to lignin. The reappearance of a band at 1738 cm^{-1} in OJF confirms that oxidation

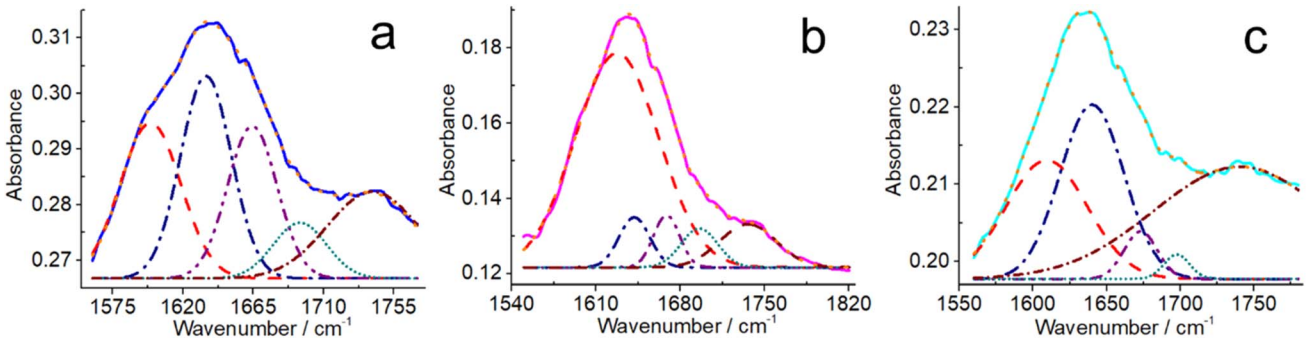

Fig. 2 Deconvoluted spectra in the region of 1550–1850 cm^{-1} for (a) OJF, (b) TJF-I, and (c) TJF-II. The solid line represents the original spectrum, and the dotted line (orange) represents the fitted curve. The dash (red), dash dot (navy), dash dot–dot (purple) short dot (dark cyan), and short dash dot (wine) lines indicate the deconvoluted spectra.

occurs in the treatment of NJF with 20% FR. The absence of bands at 1595 and 1510 cm^{-1} in OJF is ascribed to the elimination of lignin through the oxidation process. When OJF is reacted with ethanedithiol, a decrease in the intensity of the carboxylic groups at 1738 cm^{-1} for TJF-I and TJF-II is observed. This indicates a decrease in the number of carboxylic groups on the surface of TJF-I and TJF-II due to the grafting of ethanedithiol onto OJF. The characteristic band for the –S–C═O group generally appears at around 1680–1705 cm^{-1} in the spectra of TJF-I and TJF-II. However, it is not well-resolved due to the broadness of the –COOH band.

In the case of OJF, TJF-I, and TJF-II, a deconvolution method was employed to resolve the band in the range of 1550–1850 cm^{-1}, as depicted in Fig. 2. Five idiosyncratic bands are deconvoluted from the original two spectra in the above-mentioned range. The characteristic band at 1640 cm^{-1} is assigned to the –OH bending vibration of the anhydroglucose unit of cellulose. The appearance of a band at 1738 cm^{-1} is attributed to symmetric stretching of –C═O of the carboxylic group. The visualization of a characteristic new band at 1697 cm^{-1} is ascribed to the stretching vibration of the –S–C═O group of TJF-I and TJF-II after thioesterification of 20% FR-OJF.[1] This establishes that the thiol groups are anchored to the –COOH group, suggesting the transformation of the –COOH group into –CO–S–CH_2–CH_2–SH *via* thioesterification with dithiols. This is further supported by the decrease in –COOH content observed from conductometric titration.

3.3. Assessment of surface morphology

The JFs and their derivatives were examined *via* SEM analysis to study the morphology of the fibers. Fig. 3 depicts the SEM images of JF, NJF, OJF, TJF-I, and TJF-II. The SEM micrographs exhibit the effect of treatments on the fiber morphology due to the removal of lignin and hemicellulose, oxidation of the fibers, and their subsequent thioesterification with ethanedithiol. The surface of JFs is smoother than that of NJF but covered by several impurities such as hemicellulose, lignin, pectin, and waxy substances.[16] This smooth, compact structure limits the surface area available for adsorption and may hinder interfacial bonding in composites due to the presence of non-cellulosic components. The micrograph suggests that most NJF are agglomerated in certain regions due to their high specific areas and strong hydrogen bonding re-formed among the nanofibrils. In contrast, some other nanofibrils are distributed sporadically.

The NJF are rough, coarse, and not fully separated, as well as show unevenly distributed cavities on their surface. The cavities

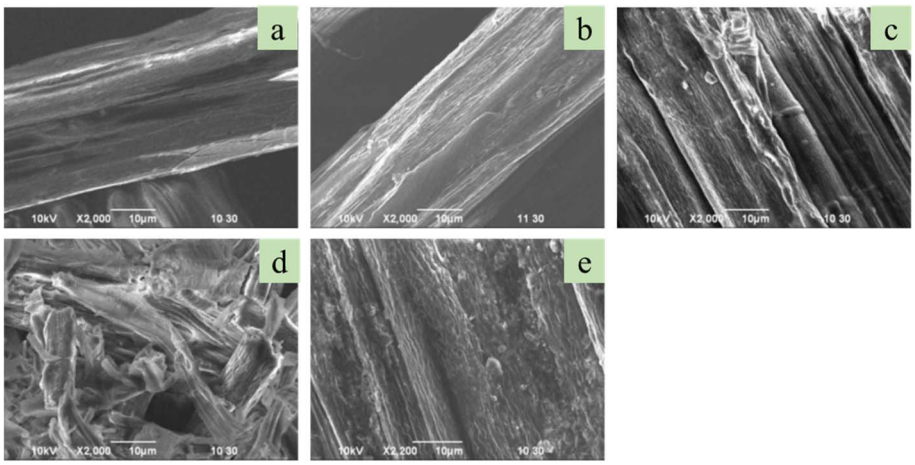

Fig. 3 SEM images of (a) JF, (b) NJF, (c) OJF, (d) TJF-I, and (e) TJF-II.

in NJF are attributed to the elimination of impurities such as hemicellulose, lignin, pectin, and waxy substances from the surface. There is a decrease in smoothness of OJF compared to NJF due to the introduction of carboxylic groups on their surface.[19] The extent of agglomeration appears to decrease due to oxidation, which increases the electrostatic repulsion as negative charges accumulate on the surface of OJF. As a result, OJF exhibits a more open and porous structure. The surfaces of TJF-I and TJF-II are different, having a comparatively heterogeneous morphology and covered with micro-sized foreign substances. These substances could be regarded as aggregates of ethanedithiol molecules incorporated by the grafting reaction. This would significantly enhance the adsorption capacity for heavy metals due to the strong binding affinity of thiols for soft metal ions (*e.g.*, Hg(II) and Cd(II)). The heterogeneous morphology with micro-sized aggregates suggests localized regions of high thiol concentration, which may act as highly efficient adsorption sites. Previous studies have shown that thiol-functionalized nanocellulose can achieve high uptake capacities for Hg(II), and similar behavior is expected for TJF-I and TJF-II.[52] Moreover, their more disordered surface aligns with the increased hydrophobicity observed in the contact angle measurements. This characteristic may enhance the selectivity for organic pollutants or non-polar dyes in wastewater treatment, given that hydrophobic surfaces preferentially adsorb non-polar molecules. The grafting of bulky thioester groups (–CO–S–CH_2–CH_2–SH) disrupts the hydrogen-bonding network and crystalline structure of cellulose, as confirmed by XRD. This increased disorder and mechanical disintegration during thioesterification further weaken the fibers. However, the increased hydrophobicity and surface functionality improve the compatibility with hydrophobic polymer matrices (*e.g.*, polyethylene and polypropylene). The rough, heterogeneous surface can enhance mechanical interlocking with polymer matrices, potentially improving the interfacial adhesion and performance of the composite in terms of flexibility and toughness, despite the lower fiber strength.

3.4. Microstate analysis

The XRD patterns of JF, NJF, OJF, TJF-I, and TJF-II are displayed in Fig. 4, which suggest that all the samples portray the characteristics of a cellulose I structure, with three peaks centered at 2θ angles of 16.5°, 22.7°, and 35.1°, corresponding to the (110), (200), and (004) lattice planes, respectively. The main peak for the (200) band at 2θ (22.8°) represents the distance between sheets of hydrogen bonding in cellulose I. The crystallinity arises from the parallel arrangement of cellulose chains, stabilized by intra- and inter-molecular hydrogen bonds. The band intensity for all the samples except JFs increases, with a slight shift in 2θ value from 22.4° to 22.6°, indicating improved crystallinity. This shift also provides evidence for the transformation of cellulose I_α into cellulose I_β after NaOH treatment, consistent with the literature.[53] Moreover, NaOH can penetrate the cellulose lattice and swell the amorphous regions. This facilitates structural rearrangement, potentially converting some cellulose I_α to the more stable cellulose I_β. The presence of hemicellulose and lignin molecules in the cellulose crystal structure of JFs probably weakens the intermolecular hydrogen bonding plane, indicating the lower intensity of JFs compared to the others.[54] The increase in the band intensity of the samples other than JFs depicts the remediation of some hemicellulose and lignin in the cellulose I structure. The new scattering peaks of cellulose II, which has a different hydrogen-bonding network and lower crystallinity, are observed after the thioesterification of OJF. The diffraction peak of cellulose I (110) ($2\theta = 15.7°$) is slightly split into cellulose II (101), corresponding to the 2θ peak position at 14.3° and cellulose I ($10\underline{1}$) ($2\theta = 16.4°$). The area under the (110) peaks of TJF-I and TJF-II is approximately 20% higher than that of other samples. Moreover, deconvolution of the peak at 15.7° was performed, and two peaks at 14.3° and 16.4° were found. The deconvoluted spectra are portrayed in Fig. 5. It is clear that during thioesterification, some parts of cellulose I (specifically I_α) are transformed into cellulose II. This transformation occurs because cellulose favors the stable structure, facilitating chain realignment after anchoring ethanedithiol onto the OJF backbone.[55]

Table 1 exhibits the values of the crystallinity index, average crystallite size, and 2θ at maximum intensity for all the samples. The crystallinity of NJF is enhanced compared to that of the pristine JFs, which is attributed to the elimination of amorphous substances such as hemicellulose, pectin, and a small portion of lignin. At certain concentrations of NaOH, the dehydrated ions can permeate the cellulose lattice because of size restrictions. The amorphous parts and surface impurities first reacted with hydrated hydroxide ions, got swelled, and detached from the JFs at the beginning of the alkalization process. Upon exposure to the aqueous alkali solution, the inter-fibrillar regions inside become less dense and rigid, enabling them to more easily rearrange spontaneously.[56] As a result, the CI of the NaOH-mediated JFs increases. This result is also consistent with a previous report, which conveyed that the crystallinity (66.08%) of NaOH-treated JFs was higher than that of pristine JFs (63.73%). The synergistic increase in crystallinity after oxidation is not solely due to the partial loss of disordered regions during washing, which are removed because of their higher water solubility. It also results from the complete removal of lignin, as confirmed by the FTIR analysis.

The crystallinity of OJF is similar to that in the previous reports on bionanowhiskers generated from JFs having

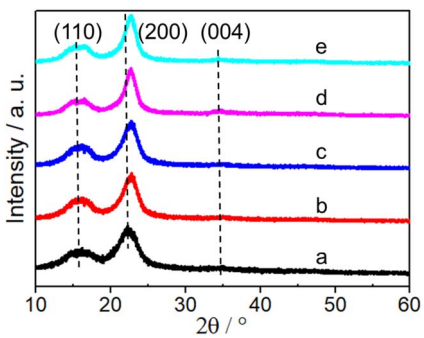

Fig. 4 XRD patterns of (a) JF, (b) NJF, (c) OJF, (d) TJF-I, and (e) TJF-II.

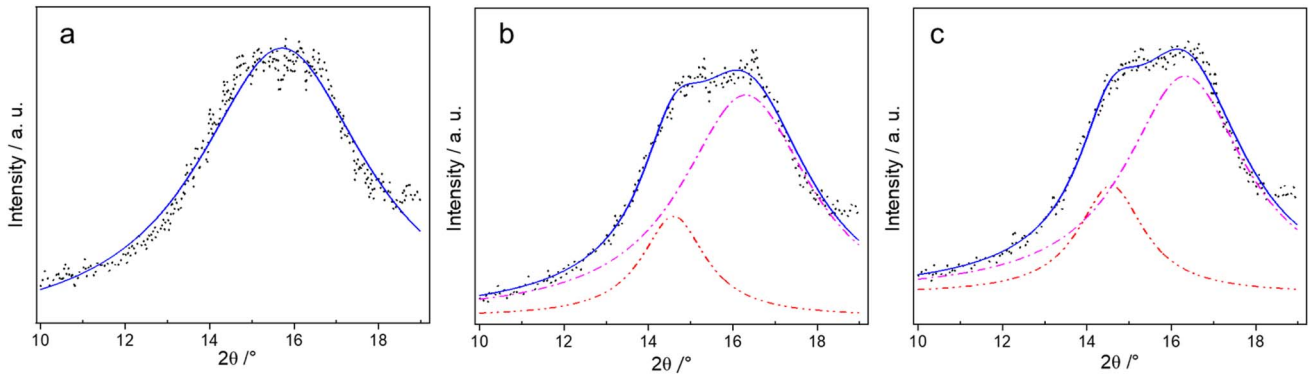

Fig. 5 Deconvoluted spectra of 10°–20° region for (a) OJF, (b) TJF-I, and (c) TJF-II. The scattered points represent the original spectrum and the solid line (blue) represents the fitted curve. The dash dot (magenta) and dash dot–dot (red) lines indicate the deconvoluted spectra.

a crystallinity of about 84.0% obtained by the acid hydrolysis method.[23] The introduction of bulky thioester groups (–S–CH_2–CH_2–SH) on the cellulose backbone disrupts the tight packing of the cellulose chains. These groups are less polar than hydroxyl or carboxyl groups, reducing the capacity for hydrogen bonding, which is critical for maintaining crystalline order. This leads to increased disorder in the crystalline regions, lowering the CI. The grafted thiol groups mitigate the fiber cross-sectional dimensions and generate localized amorphous regions on the surface of the fibers by the coupling of ethanedithiol to the anhydroglucoronic unit of OJF. SEM observations of a heterogeneous morphology and micro-sized aggregates in TJF-I and TJF-II support this consideration. This is analogous to other surface modifications, such as silanization, where the CI of hemp fibers decreased to 59% due to the formation of an amorphous layer.[57] The mechanical disintegration and chain scission, as evidenced by the brittleness of TJF-I and TJF-II, may disrupt the crystalline domains, further contributing to the CI assuagement.

The XRD data align with the FTIR and conductometric titration results, confirming that thioesterification reduces the ordered hydrogen-bonding network by replacing –COOH with –CO–S–CH_2–CH_2–SH. The crystallite size remains relatively stable (5.14–6.46 nm across samples), suggesting that the decrease in crystallinity is primarily due to the increase in amorphous regions rather than a reduction in crystallite dimensions. The partial transformation to cellulose II and decreased CI improve the flexibility and reactivity of the fibers. These changes make the fibers suitable for applications such as heavy metal remediation and composite reinforcement, where surface functionality and compatibility with hydrophobic matrices are essential.

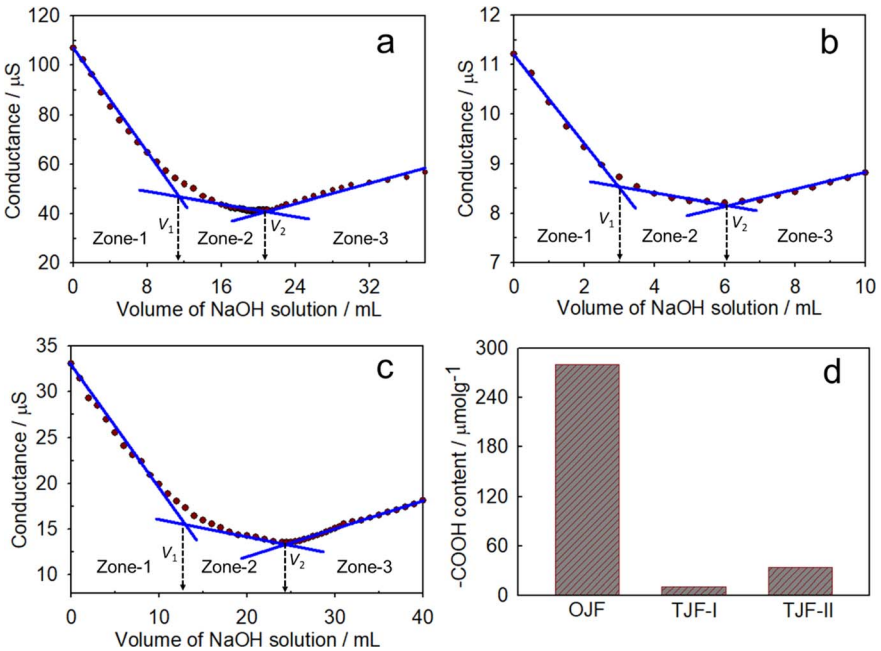

Fig. 6 Conductometric titration curves of (a) OJF, (b) TJF-I and (c) TJF-II and (d) comparison of the surface –COOH content.

3.5. Degree of functionalization of fiber surface

The conductometric titration curves of OJF, TJF-I, and TJF-II are depicted in Fig. 6. These results were further analyzed to quantitatively determine the degree of functionalization of the surface of JFs as well as to assess the conversion of the –COOH group to –CO–S–CH_2–CH_2–. The content of carboxylic groups in OJF, TJF-I, and TJF-II was 280.39, 10.83, and 33.54 μmol g^{-1}, respectively. In the case of TJF-I and TJF-II, the content of carboxylic groups significantly decreased compared that of OJF. This mitigation in carboxylic groups was assigned to the grafting of ethanedithiol onto OJF. The content of ethanedithiol groups introduced in TJF-I and TJF-II was 269.56 and 246.85 μmol g^{-1} of dry OJF, respectively. Method I was comparatively more efficient for the incorporation of ethanedithiol on the fibers compared to Method II. Similarly, the decline in the number of carboxylic groups was used as evidence for the confirmation of grafting modification of the fibers in previous reports.[1,58]

Table 1 presents the carboxylic content and DS in the oxidized and thioesterified JFs. The DS of OJF, TJF-I, and TJF-II is 4.5%, 4.3%, and 4.0%, respectively. The DS depends on the various types of cellulose sources and the process of extraction from non-wood plants.[46] The DS for the NCO-functionalization of cellulose derived from JFs was determined to be 5.0%. In comparison, the DS of methylcellulose prepared from unbleached jute pulp reached approximately 29.0% after 3 h reaction time.[59,60]

3.6. Thermal stability analysis

Fig. 7 represents the TGA curves of JF, NJF, OJF, TJF-I, and TJF-II. All the curves showed an initial small drop between 30 °C to 150 °C, which represents weight loss due to absorbed moisture on the surface of these materials including chemisorbed water and/or intermolecular H-bonded water. The initial change near 270 °C is attributed to the decomposition of hemicellulose and lignin of JFs.[13] The decomposition temperature of the raw, extracted, oxidized and thioesterified JFs is represented in Table 1. Thermal degradation of JFs and NJF starts at approximately 270 °C in an N_2 atmosphere, while in the case of OJF degradation, it begins at approximately 235 °C. Thus, the formation of carboxylate groups on the cellulose microfibril surfaces of OJF by oxidation leads to a significant reduction in its thermal degradation point.[61] The β glycosidic linkage was broken during the oxidation process, which led to a shortening in the chain length of the cellulose molecules in JFs. The larger surface area of OJF is exposed to heat, which facilitates heat transfer and lowers the decomposition temperature of OJF. Likewise, the increased polarity of –COOH groups also enhances heat transfer, accelerating its degradation. It is worth mentioning that the decomposition shifts to 250 °C for TJF-I, which is greater than that of OJF. This confirms the grafting of ethanedithiol onto OJF. The thioester bond (C–S–C) is less polar and more thermally stable than –COOH, given that it is less prone to decarboxylation. This contributes to the improved thermal stability of TJF-I compared to OJF. The thiol group (–SH) is relatively stable at moderate temperatures but can undergo oxidation or desulfurization above 300 °C, influencing the degradation profile. Furthermore, thiol groups are less polar than hydroxyl (–OH) or carboxyl groups, reducing the capacity of the fibers for hydrogen bonding and water retention.

The TGA curves show a lower weight loss (30–150 °C) for TJF-I and TJF-II due to the reduced moisture content, reflecting an increase in hydrophobicity. The thermal degradation of TJF-II commenced at 230 °C, which is slightly lower compared to that of OJF.[62] This is because of the mechanical disintegration of TJF-II during its synthesis process, which enhances its surface area. The improved thermal stability of TJF-I, and to some extent in TJF-II indicates that the modified fibers are more resistant to thermal degradation. The enhanced stability is attributed to the formation of thermally stable thioester bonds and reduced presence of thermally labile hemicellulose. This enhances their longevity in end-use applications, especially in moderate thermal stress environments. TGA revealed the differences in the thermal stability of TJF-I and TJF-II, which both underwent thioesterification but with varying treatment and reagent concentrations. TJF-I showed slightly higher thermal stability compared to TJF-II, which is likely due to the higher number of thiol groups and formation of thermally stable intermediates by sulfur in the thioester and thiol groups. This result is also supported by conductometric titration and contact angle measurements. The enhanced stability is

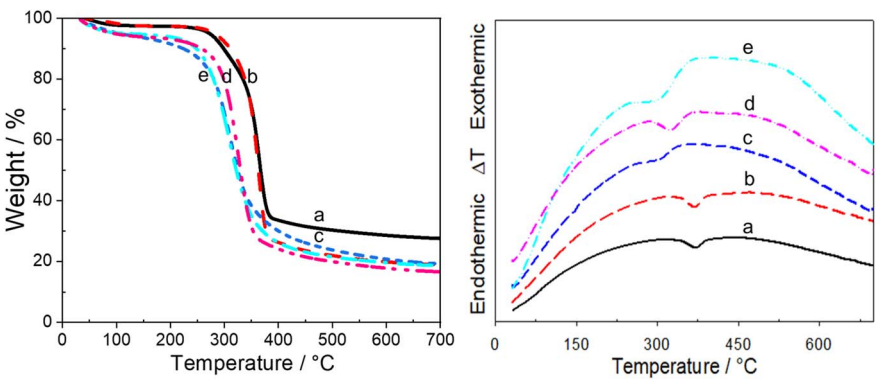

Fig. 7 (i) TGA and (ii) DTA curves of (a) JF, (b) NJF, (c) OJF, (d) TJF-I, and (e) TJF-II.

attributed to the formation of thermally stable thioester bonds and reduced presence of thermally labile hemicellulose.

The DTA curves measured for JFs, NJF, OJF, TJF-I, and TJF-II are shown in Fig. 7. The DTA curves of JFs and NJF reveal a sharp endothermic peak at 368 °C for the decomposition of the crystalline part of cellulose in JFs. The decomposition of OJF shifted to a lower temperature at 310 °C, which indicates a decrease in the thermal stability of OJF. The degradation band of TJF-I appeared at 330 °C. Alternatively, the degradation of TJF-II occurred at 295 °C, which is slightly lower than that of OJF because of the mechanical disintegration of TJF-II during its synthesis. Additional evidence of ethanedithiol coupling onto OJF is obtained from the decomposition behavior of TJF-II, given that the decomposition temperature of TJF-II is higher compared to that of OJF. The increased thermal resistance of TJF-I, and to a lesser extent of TJF-II suggests their suitability for processing with polymers that require elevated temperatures, such as composite extrusion, compression molding, and film casting. This widens the application scope of the modified jute fibers in industries such as automotive, construction, and packaging.

3.7. Assessment of fiber strength

The bundle strength of the JFs, NJF, and OJF was 1.13, 1.02, and 0.07 lb mg^{-1}, respectively. The decline in the strength of NJF corresponds to the removal of hemicellulose, lignin, and pectin from the fibers. This is consistent with the literature, where a decrease in fiber strength was reported when JFs were treated with NaOH, resulting in the removal of waxing and lignin from the fibers.[44,63] The fiber strength of OJF is lower than that of NJF owing to the introduction of –COOH groups on the fiber surface. The bundle strength of TJF-I and TJF-II could not be determined because these fibers were very brittle and defibrillated. To examine the effect of solvents on the fibers, JFs, NJF, and OJF were treated with a mixture of toluene, water, and acetonitrile at 85 °C and 40 °C, respectively. In both cases, these fibers are as brittle as TJF-I and TJF-II. This suggests that the brittleness in the fibers of TJF-I and TJF-II could be attributed to the introduction of thiol groups in the cellulose moiety. The brittleness observed in TJF-I and TJF-II is attributed to mechanical disintegration during thioesterification, and may be advantageous in applications requiring high surface area and flexibility, such as dispersible adsorbents.

3.8. Surface wettability

A higher contact angle value of a sample in water indicates its more hydrophobic nature, whereas a lower contact angle value in organic solvents designates the more hydrophobic nature of the substance. The contact angles of JFs, NJF, OJF, TJF-I, and TJF-II are 6.58°, 4.79°, 4.67°, 2.48° and 4.5°, respectively. In general, these contact angle values are relatively low, given that the medium was a mixture of toluene and water. However, as cellulose is cemented with hemicellulose and lignin, it is hydrophilic in nature and exhibits a higher contact angle value. Upon NaOH treatment, all the hemicellulose and some amount of lignin are removed and a decrease in contact angle is observed for NJF. The contact angle for OJF prepared by oxidation remains almost the same. The removal of the rest of the lignin and introduction of carboxylic groups during oxidation act in the counter direction and the contact angle of OJF is not affected. The removal of some amount of lignin by alkali treatment and all the lignin by oxidation is also supported by the FTIR analysis. The contact angle of TJF-I and TJF-II significantly decreased compared to OJF. This is attributed to the increase in hydrophobicity due to the anchoring of ethylenedithiol onto OJF by esterification. In terms of practical application, the reduced hydrophilicity of these samples has several implications in composite materials including enhanced hydrophobicity improves the compatibility with hydrophobic polymer matrices, such as polyethylene and polypropylene. This can lead to better fiber dispersion, improved interfacial adhesion, and ultimately enhanced mechanical properties in the resulting biocomposites. Furthermore, the decrease in water uptake due to reduced hydrophilicity can improve the dimensional stability and durability of fiber-reinforced materials, especially in humid or aqueous environments. It has been reported that a pure cellulose sample displayed a lower contact angle value (42.2°) in water, while JFs comprising non-cellulosic substances such as lignin, hemicellulose and pectin have a higher value (65.7°) in water, unveiling their poorer hydrophilic character.[64] In another study, it has been revealed that jute and soy resin are hydrophilic in nature, having contact angle values in water of 42.1° and 50.4°, respectively. Woven jute soy exhibited a contact angle value in water of 63.5°, corresponding to the more hydrophobic nature of this sample.[65]

3.9. Prospects of the modified jute fibers in environmental pollution control

The thioesterification of JFs introduces thiol (–SH) groups onto their cellulose backbone, significantly enhancing their adsorption properties for heavy metal ions and organic pollutants. The successful grafting, as confirmed by FTIR (new thioester band at 1697 cm^{-1}) and conductometric analysis, endows these fibers with exceptional potential for environmental applications. The introduction of thiol groups *via* thioesterification enhances the adsorption capacity of JFs by providing highly reactive sites for soft metal ions, such as Hg(II), Cd(II), and Pb(II), according to the hard-soft acid–base (HSAB) theory. The sulfur atom in the –SH group forms stable coordination complexes with these metals through chelation or ion exchange, as evidenced by the high thiol content in TJF-I and TJF-II. SEM analysis reveals a heterogeneous surface morphology with micro-sized aggregates, increasing the effective surface area and accessibility of the adsorption sites. The decreased crystallinity and partial transformation from cellulose I to cellulose II further enhance the functional group accessibility, facilitating metal ion interactions. Comparatively, Geng *et al.* reported a thiol-functionalized nanocellulose aerogel with an Hg(II) adsorption capacity of ~280 mg g^{-1}, driven by a high density of thiol groups introduced *via* 3-mercaptopropyltrimethoxysilane. The thiol content in TJF-I (269.56 μmol g^{-1}) suggests a theoretical Hg(II) adsorption capacity of ~270 mg g^{-1} (assuming 1 : 1 binding

stoichiometry), which is competitive with these results.[52] Similarly, thiol-modified cellulose nanofibers have been studied, exhibiting adsorption capacities of 112 mg g^{-1} for Cr(VI) and 84 mg g^{-1} for Pb(II), which is attributed to their increased surface accessibility and thiol availability.[66] Compared to non-cellulosic adsorbents, such as activated carbon (Hg(II) capacity of 50–200 mg g^{-1}), thiol-grafted JFs offer superior sustainability and cost-effectiveness.[67] The eco-friendly synthesis using the Fenton reagent, which produces water and oxygen as by-products, contrasts with energy-intensive activated carbon production or costly TEMPO-based oxidation methods.[37,61] The increased hydrophobicity of TJF-I and TJF-II also enhances their compatibility with non-polar pollutants, such as organic dyes, broadening their applicability in complex wastewater matrices.

The strong affinity of thiol groups for soft metal ions positions TJF-I and TJF-II as effective adsorbents for Hg(II), Cd(II), and Pb(II) in industrial effluents, mining runoff, and contaminated groundwater. Their theoretical adsorption capacity, which is comparable to thiol-functionalized nanocellulose, suggests their efficacy in removing toxic metals from water sources.[52] TJF-I and TJF-II have a high degree of substitution (DS of 4.3–4.5%), with residual carboxyl groups in TJF-II, suggesting dual functionality in multi-pollutant systems. They can adsorb cationic and anionic pollutants in applications such as fixed-bed columns, filtration membranes, and dispersible adsorbents, while being biodegradable. The increased hydrophobicity and surface heterogeneity of TJF-I and TJF-II make them suitable for adsorbing organic dyes, such as methylene blue and disperse dyes, which are common in textile effluents. The thiol groups can interact with cationic dyes *via* electrostatic forces, while hydrophobic interactions capture non-polar dyes, as supported by Yang *et al.* (2014).[66] Their alleviated hydrophilicity minimizes swelling, improving their stability in filtration systems. Compared to activated carbon, jute-based adsorbents are renewable and cost-effective, leveraging abundant jute resources in regions such as Bangladesh and India.[12] TJF-I and TJF-II can be applied as soil amendments to immobilize heavy metals, preventing their leaching into groundwater. Furthermore, their thiol groups form stable complexes with metals, reducing their bioavailability and environmental risk.

4. Conclusions

In this study, a new method was presented for grafting thiol compounds in JFs, which were pretreated with an alkali solution, followed by an oxidation reaction. Hemicellulose seemed much easier to remove by the alkalization process compared to lignin. The alkali treatment effectively removed hemicellulose, as evidenced by the disappearance of its FT-IR band at 1738 cm^{-1}, while lignin was partially retained, as confirmed by its FT-IR peaks at 1502 and 1030 cm^{-1}. Oxidation with 20% Fenton reagent introduced a significant amount of carboxylic groups (280.39 μmol g^{-1}), which decreased post-thioesterification, confirming the successful grafting of ethanedithiol onto the cellulose backbone. The presence of the thioester bond (C═O–S) was indicated by a new FT-IR band at 1697 cm^{-1}. X-ray diffraction revealed a partial transformation from cellulose I to cellulose II in TJF-I and TJF-II, with a slight reduction in the crystallinity index, reflecting the increased disorder due to bulky thiol groups. SEM analysis showed their heterogeneous morphology with micro-sized aggregates, enhancing their adsorption potential. The decrease in contact angle, caused by the increased hydrophilicity, further confirmed the successful incorporation of thiol into the cellulose moiety. This modification improves the compatibility with hydrophobic polymer matrices for composite applications by enhancing the interfacial adhesion. Thermal stability improved in TJF-I compared to OJF, which is attributed to its stable thioester bonds. The brittleness observed in TJF-I and TJF-II, due to mechanical disintegration, suggests their suitability for high-surface-area applications such as dispersible adsorbents. The thus-synthesized JF derivative containing the thioester group display potential for environmental applications such as the removal of heavy metals, industrial dyes, and wastewater treatment. The method described herein for grafting could potentially be extended to functionalize other natural cellulose-based materials with a high cellulose content. This work demonstrates a simple, one-step thioesterification route for JFs that introduces thiol groups with potential for further functionalization, alongside improved thermal and surface properties. These features position this material as a more versatile candidate for composite and functional material applications compared to conventional modifications. Thus, the thiol-grafted JFs exhibit significant potential for environmental applications, particularly in wastewater treatment and heavy metal remediation, due to their high thiol content and heterogeneous surface morphology.

Author contributions

Md. Sadiqul Islam Sheikh: methodology, investigation, visualization, formal analysis, writing – original draft; Md. Rezanur Rahman: methodology, visualization, peer support; Muhammed Shah Miran: validation, review & editing, project administration; Md. Abu Bin Hasan Susan: resources, writing – review & editing, Md. Mominul Islam: conceptualization, resources, writing – review & editing, funding acquisition, visualization, supervision.

Conflicts of interest

The authors declare that they have no known competing financial interests or personal relationships that could have appeared to influence the work reported in this paper.

Data availability

The data supporting this article has been included in the main manuscript and supplementary information (SI). Supplementary information is available. See DOI: **https://doi.org/10.1039/d5ra07729j**.

Acknowledgements

The financial support from the University of Dhaka and the University Grants Commission of Bangladesh is greatly acknowledged. The Fibers and Polymers Research Division, BCSIR Laboratories, Dhaka, is highly appreciated for providing the support of bundle strength measurement.

References

1 M. S. I. Sheikh, M. S. Miran, M. A. B. H. Susan and M. M. Islam, *Carbohydr. Polym. Technol. Appl.*, 2024, **7**, 100608, DOI: **10.1016/j.carpta.2024.100608**.
2 M. M. Islam, M. S. I. Sheikh, M. A. B. H. Susan and M. M. Islam, in *Organic Electrodes*, Springer, 2022, pp. 265–287, DOI: **10.1007/978-3-030-98021-4_15**.
3 S. S. Nair, J. Zhu, Y. Deng, *et al.*, *Sustainable Chem. Processes*, 2014, **2**, 23, DOI: **10.1186/s40508-014-0023-0**.
4 Y. Habibi, L. A. Lucia and O. J. Rojas, *Chem. Rev.*, 2010, **110**, 3479–3500, DOI: **10.1021/cr900339w**.
5 S. J. Eichhorn, A. Dufresne, M. Aranguren, *et al.*, *J. Mater. Sci.*, 2010, **45**, 1–33, DOI: **10.1007/s10853-009-3874-0**.
6 T. Hirano, K. Mitsuzawa, S. Ishioka, K. Daicho, H. Soeta, M. Zhao and T. Saito, *Front. Chem.*, 2020, **8**, 68, DOI: **10.3389/fchem.2020.00068**.
7 M. A. Hubbe, J. S. Daystar, R. A. Venditti, J. J. Pawlak, M. C. Zambrano, M. Barlaz and S. Pires, *Bioresources*, 2025, **20**, 1, DOI: **10.15376/biores.20.1.hubbe**.
8 H. Zhu, W. Luo, P. N. Ciesielski, Z. Fang, J. Y. Zhu, G. Henriksson, M. E. Himmel and L. Hu, *Chem. Rev.*, 2016, **116**, 9305–9374, DOI: **10.1021/acs.chemrev.6b00225**.
9 M. Z. Hassan, M. S. I. Sheikh, P. Ahamed and M. A. Yousuf, *Carbohydr. Polym. Technol. Appl.*, 2025, **10**, 100751, DOI: **10.1016/j.carpta.2025.100751**.
10 M. S. I. Sheikh, M. M. Islam, M. S. Hossain and M. M. Islam, in *Specialty Polymers: Fundamentals, Properties, Applications and Advances*, CRC Press, 2023, pp. 185–201.
11 C. Zequine, C. K. Ranaweera, Z. Wang, P. R. Dvornic, P. K. Kahol, S. Singh, P. Tripathi, O. N. Srivastava, S. K. Singh and R. K. Gupta, *Sci. Rep.*, 2017, **7**, 1174, DOI: **10.1038/s41598-017-01319-w**.
12 X. Cao, B. Ding, J. Yu and S. S. Al-Deyab, *Carbohydr. Polym.*, 2012, **90**, 1075–1080, DOI: **10.1016/j.carbpol.2012.06.046**.
13 T. S. Kumar, S. S. Kumar and L. R. Kumar, in *Plant Fibers, Their Composites, and Applications*, Woodhead Publishing, 2022, pp. 253–282, DOI: **10.1016/B978-0-12-824528-6.00020-5**.
14 A. Rahman, M. A. Chowdhury, M. B. A. Shuvho, N. Hossain, M. Fotouhi and R. Ali, *Polym. Bull.*, 2022, **79**, 1–27, DOI: **10.1007/s00289-021-04049-2**.
15 A. Farooq, S. R. Islam, M. Al-Amin, M. K. Patoary, M. T. Hossain, M. T. Khawar and S. M. A. K. Shah, *Carbohydr. Polym.*, 2024, **324**, 122423, DOI: **10.1016/j.carbpol.2024.122423**.
16 J. Lin, L. Yu, F. Tian, N. Zhao, X. Li, F. Bian and J. Wang, *Carbohydr. Polym.*, 2014, **109**, 35–43, DOI: **10.1016/j.carbpol.2014.03.045**.
17 L. Y. Mwaikambo, *Afr. J. Sci. Technol.*, 2006, **7**, 120–133.
18 K. Das, D. Ray, C. Banerjee, N. R. Bandyopadhyay, S. S. Sahoo, A. K. Mohanty and M. Misra, *Ind. Eng. Chem. Res.*, 2010, **49**, 2775–2782, DOI: **10.1021/ie9019984**.
19 L. Yu, J. Lin, F. Tian, X. Li, F. Bian and J. Wang, *J. Mater. Chem. A*, 2014, **2**, 6402–6411, DOI: **10.1039/c4ta00004h**.
20 H. Wang, L. Huang and Y. Lu, *Fibers Polym.*, 2009, **10**, 442–445, DOI: **10.1007/s12221-009-0442-9**.
21 M. M. Bashar, H. Zhu, S. Yamamoto and M. Mitsuishi, *Cellulose*, 2019, **26**, 3671–3684, DOI: **10.1007/s10570-019-02363-7**.
22 M. S. Jahan, A. Saeed, Z. He and Y. Ni, *Cellulose*, 2011, **18**, 451–459, DOI: **10.1007/s10570-010-9481-z**.
23 N. Kasyapi, V. Chaudhary and A. K. Bhowmick, *Carbohydr. Polym.*, 2013, **92**, 1116–1123, DOI: **10.1016/j.carbpol.2012.10.021**.
24 M. M. Huque, M. Habibuddowla, A. J. Mahmood and A. J. Mian, *J. Polym. Sci., Polym. Chem. Ed.*, 1980, **18**, 1447–1458, DOI: **10.1002/pol.1980.170180502**.
25 A. K. Mohanty, S. Patnaik, B. C. Singh and M. Misra, *J. Appl. Polym. Sci.*, 1989, **37**, 1171–1181, DOI: **10.1002/app.1989.070370502**.
26 I. H. Mandal, *J. Eng. Fibers Fabr.*, 2013, **8**, 42–50, DOI: **10.1177/155892501300800305**.
27 A. Dong, K. M. Teklu, W. Wang, X. Fan, P. Wang, Y. Hou and C. Yu, *Int. J. Biol. Macromol.*, 2020, **160**, 192–200, DOI: **10.1016/j.ijbiomac.2020.05.167**.
28 S. Moharana and S. S. Tripathy, *J. Appl. Polym. Sci.*, 1991, **42**, 1001–1008, DOI: **10.1002/app.1991.070420414**.
29 N. Gibeop, D. W. Lee, C. V. Prasad, F. Toru, B. S. Kim and J. I. Song, *Adv. Compos. Mater.*, 2013, **22**, 389–399, DOI: **10.1080/09243046.2013.843814**.
30 M. A. Khan, M. S. Rahaman, A. Al-Jubayer and J. M. M. Islam, in *Cellulose-Based Graft Copolymers: Structure and Chemistry*, CRC Press, 2015, pp. 209–236.
31 A. Jha, A. Thite, S. R. Chowdhury, Y. K. Bhardwaj and H. J. Pant, *J. Appl. Polym. Sci.*, 2023, **140**, e54690, DOI: **10.1002/app.54690**.
32 M. M. Hassan, M. R. Islam, S. Shehrzade and M. A. Khan, *Polym.-Plast. Technol. Eng.*, 2003, **42**, 515–531, DOI: **10.1081/PPT-120023092**.
33 N. Pal, S. Banerjee, P. Roy and K. Pal, *Mater. Sci. Eng., C*, 2019, **104**, 109956, DOI: **10.1016/j.msec.2019.109956**.
34 R. Acosta Ortiz, R. Yañez Macías, J. D. J. Ku Herrera and A. E. García Valdez, *Polymers*, 2022, **15**, 60, DOI: **10.3390/polym15010060**.
35 H. Wu, C. Silva, Y. Yu, A. Dong, Q. Wang, X. Fan and A. Cavaco-Paulo, *New J. Chem.*, 2017, **41**, 3773–3780, DOI: **10.3390/polym15010060**.
36 A. M. El-Shafei, A. M. Adel, A. A. Ibrahim and M. T. Al-Shemy, *Int. J. Biol. Macromol.*, 2019, **124**, 733–741, DOI: **10.1016/j.ijbiomac.2018.11.180**.
37 M. S. Hossain, M. Y. Pabel and M. M. Islam, in *Advanced Oxidation Processes in Dye-Containing Wastewater*, Springer, 2022, pp. 29–89, DOI: **10.1007/978-981-19-0882-8_2**.
38 R. Saravanan, J. A. Solairaju, T. Sathish, J. Giri and M. I. Ammarullah, *Eng. Rep.*, 2024, **7**(1), e13059, DOI: **10.1002/eng2.13059**.

39 M. D. Teli and S. P. Valia, *Fibers Polym.*, 2013, **14**, 915–919, DOI: 10.1007/s12221-013-0915-8.
40 C. K. Hong, N. Kim, S. L. Kang, C. Nah, Y.-S. Lee, B.-H. Cho and J.-H. Ahn, *Plast, Rubber Compos.*, 2008, **37**, 325–330, DOI: 10.1179/174328908X314334.
41 M. S. Hassan and M. H. Zohdy, *J. Vinyl Addit. Technol.*, 2018, **24**, 339–346, DOI: 10.1002/vnl.21571.
42 S. Iimura, K. Manabe and S. Kobayashi, *Chem. Commun.*, 2002, 94–95, DOI: 10.1039/b109834a.
43 A. S. El-Azab and A. A.-M. Abdel-Aziz, *Phosphorus, Sulfur Silicon Relat. Elem.*, 2012, **187**, 1046–1055, DOI: 10.1080/10426507.2012.664220.
44 M. R. Rahman, M. S. I. Sheikh, M. S. Miran, M. M. Alamgir, M. A. B. H. Susan and M. M. Islam, *Bangladesh J. Sci. Res.*, 2020, **33**, 66–72.
45 Y. Habibi, H. Chanzy and M. R. Vignon, *Cellulose*, 2006, **13**, 679–687, DOI: 10.1007/s10570-006-9075-y.
46 Z. Tang, W. Li, X. Lin, H. Xiao, Q. Miao, L. Huang, L. Chen and H. Wu, *Polymers*, 2017, **9**, 421, DOI: 10.3390/polym9090421.
47 P. R. Sharma, R. Joshi, S. Sharma and B. S. Hsiao, *Biomacromolecules*, 2017, **18**, 2333–2342, DOI: 10.1021/acs.biomac.7b00544.
48 E. Sinha and S. K. Rout, *Bull. Mater. Sci.*, 2009, **32**, 65–76, DOI: 10.1007/s12034-009-0010-3.
49 X. Wang, L. Chang, X. Shi and L. Wang, *Materials*, 2019, **12**, 1386, DOI: 10.3390/ma12091386.
50 T. Hosoya, M. Bacher, A. Potthast, T. Elder and T. Rosenau, *Cellulose*, 2018, **25**, 3797–3814, DOI: 10.1007/s10570-018-1835-y.
51 D. Ray and B. K. Sarkar, *J. Appl. Polym. Sci.*, 2001, **80**, 1013–1020, DOI: 10.1002/app.1184.
52 B. Geng, H. Wang, S. Wu, J. Ru, P. Tong, Y. Wang and W. Chen, *ACS Sustainable Chem. Eng.*, 2017, **5**, 11715–11726, DOI: 10.1021/acssuschemeng.7b03188.
53 M. Wada, T. Okano and J. Sugiyama, *J Wood Sci.*, 2001, **47**, 124–128, DOI: 10.1007/BF00780560.
54 P. R. Sharma, P. R. Rajamohanan and A. J. Varma, *Carbohydr. Polym.*, 2014, **113**, 615–623, DOI: 10.1016/j.carbpol.2014.07.056.
55 D. Klemm, B. Heublein, H. P. Fink and A. Bohn, *Angew. Chem., Int. Ed.*, 2005, **44**, 3358–3393, DOI: 10.1002/anie.200460587.
56 M. H. Lee, H. S. Park, K. J. Yoon and P. J. Hauser, *Text. Res. J.*, 2004, **74**, 146–154, DOI: 10.1177/004051750407400211.
57 U. Moonart and S. Utara, *Cellulose*, 2019, **26**, 7271–7295, DOI: 10.1007/s10570-019-02611-w.
58 E. Zhao, Y. Repo, D. Song, Y. Yin, S. B. Peralta and Y. Zhang, *Green Chem.*, 2017, **19**, 4816–4828, DOI: 10.1039/c7gc01770g.
59 R. Gallego, C. C. Piras, L. A. J. Rutgeerts, A. Fernandez-Prieto and M. E. G. Mosquera, *Cellulose*, 2020, **27**, 643–656, DOI: 10.1007/s10570-019-02831-0.
60 S. A. Ria, T. Ferdous, K. M. Y. Arafat and M. S. Jahan, *Biomass Convers. Biorefin.*, 2022, **12**, 2431–2439, DOI: 10.1007/s13399-020-00741-x.
61 A. Isogai, T. Saito and H. Fukuzumi, *Nanoscale*, 2011, **3**, 71–85, DOI: 10.1039/C0NR00583E.
62 P. Lu and Y.-L. Hsieh, *Carbohydr. Polym.*, 2010, **82**, 329–336, DOI: 10.1016/j.carbpol.2010.04.073.
63 S. Aziz, M. Ansell, S. Clarke and S. Panteny, *Compos. Sci. Technol.*, 2005, **65**, 525–535, DOI: 10.1016/j.compscitech.2004.08.005.
64 L. Serrano, I. Urruzola, D. Nemeth, K. Belafi-Bako and J. Labidi, *Desalination*, 2011, **270**, 143–150, DOI: 10.1016/j.desal.2010.11.038.
65 A. K. Behera, S. Avancha, R. K. Basak, R. Sen and B. Adhikari, *Carbohydr. Polym.*, 2012, **88**, 329–335, DOI: 10.1016/j.carbpol.2011.12.023.
66 R. Yang, K. B. Aubrecht, H. Ma, R. Wang, R. B. Kim, J. Wang, H. Yu and J. Wang, *Polymer*, 2014, **55**, 1167–1176, DOI: 10.1016/j.polymer.2014.01.043.
67 P. Hadi, M. Xu, C. Ning, C. S. K. Lin and G. McKay, *Chem. Eng. J.*, 2015, **260**, 895–906, DOI: 10.1016/j.cej.2014.08.088.